Physica D 308 (2015) 80–86

Contents lists available at ScienceDirect

Physica D

journal homepage: www.elsevier.com/locate/physd

Nonlinear conductance and heterogeneity of voltage-gated ion channels allow defining electrical surface domains in cell membranes

Javier Cervera *, José A. Manzanares, Salvador Mafe

Departament de Termodinàmica, Universitat de València, E-46100 Burjassot, Spain

HIGHLIGHTS

- Spatial domains of different electrical characteristics coexist on the cell surface.
- A phenomenological model for voltage-gated channels over the cell membrane is used.
- Channels of distinct characteristics induce different sensitivities over the membrane.
- Domains of different properties locally modulate electrical signals over the membrane.

GRAPHICAL ABSTRACT

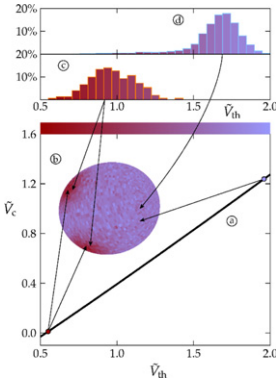

Heterogeneity in the channel threshold potentials allows defining a spatial map over a model cell membrane.

ARTICLE INFO

Article history:
Received 21 January 2015
Received in revised form
6 May 2015
Accepted 30 May 2015
Available online 6 June 2015
Communicated by K. Josic

Keywords:
Cell membrane
Ion channel
Threshold potential
Heterogeneity
Bioelectrical signals

ABSTRACT

The membrane potential of a cell measured by typical electrophysiological methods is only an average magnitude and experimental techniques allowing a more detailed mapping of the cell surface have shown the existence of spatial domains with locally different electric potentials and currents. Electrical potentials in non-neural cells are regulated by the nonlinear conductance of membrane ion channels. Voltage-gated potassium channels participate in cell hyperpolarization/depolarization processes and control the electrical signals over the cell surface, constituting good candidates to study basic biological questions on a more simplified scale than the complex cell membrane. These channels show also a high heterogeneity, making it possible to analyze the effects of diversity in the electrical responses of channels localized on spatial domains. We use a phenomenological approach of voltage gating that reproduces the observed rectification characteristics of inward rectifying potassium channels and relate the threshold voltage heterogeneity of the channels to the establishment of spatial domains with different electrical sensitivities. Although our model is only a limited picture of the whole cell membrane, it shows that domains with different ion channels may permit or suppress steady state bioelectrical signals over the cell surface according to their particular voltage sensitivity. Also, the nonlinear electrical coupling of channels with different threshold potentials can lead to a rich variety of bioelectrical phenomena, including regions of membrane potential bi-stability.

* Corresponding author. Tel.: +34 96 3543926.
E-mail address: javier.cervera@uv.es (J. Cervera).

http://dx.doi.org/10.1016/j.physd.2015.05.017
0167-2789/

1. Introduction

1.1. Electrical signals in cells and ion channels

Electric potentials and currents are characteristic of cells and tissues. The coupling of the membrane potential, defined as the electrical potential difference between the cytoplasm and the extracellular environment at zero current, to ionic gradients allows nonlinear signaling pathways essential to the cell cycle, tissue morphogenesis and wound regeneration, cancer progress, and the regulation of the left–right asymmetry [1–4]. Electrical signals in the cell are usually supported by ion channels, blockers, and transporters localized over heterogeneous patches of the membrane surface [4,5]. These channels can control cell cycle progression [6] and patterning [7,8] because electric potential gradients act in concert with specific ligand–receptor instructions. As opposed to the action potential of neurons, electrical potentials in non-neural cells show slow changes along the cell cycle that may be related to changes in the nonlinear conductance of ion channels [4,6]. In particular, the membrane potential constitutes an average magnitude resulting from the individual activity of ion channels and transporters with different electric characteristics localized over cell surface domains (see [9,10] and references therein).

Although biological processes typically require the coordinated action of many channels and pumps, potassium channels play a pivotal role because they regulate the membrane potential [5,6], controlling the cell cycle and cancer progression by means of ionic conduction and permeation-independent mechanisms [6,11,12]. Indeed, voltage-gated potassium channels participate in cell hyperpolarization and depolarization processes, control the driving force for the entry of calcium ions into the cell triggering different intracellular signals, and regulate electrical signals over localized domains of the cell surface, providing also relevant positional information [4–6,9,13]. In this study, we concentrate mostly on the electrical characteristics of the inward rectifying channels because of their generality and significant role in cell biology [6,7,14,15].

1.2. Electrical characteristics of voltage-gated ion channels

The inward rectifying potassium channels form a heterogeneous group [6,7,14,15] that may conduct large inward currents at potentials more negative than the equilibrium Nernst potential E_{in} (hyperpolarization) and low outward currents at potentials less negative than E_{in} (depolarization) [5]. The equilibrium potentials correspond to the logarithm of the ratio of the ionic concentrations in the extracellular medium and the cytoplasm [5]. Fig. 1(a) shows the essential nonlinear characteristics of these channels, reproduced by the phenomenological current (I)–potential (V) curve [5,15–17]:

$$I = G(V - E_{in})P_{open}(V),$$

$$P_{open}(V) = \frac{1}{1 + \exp[zF(V - V_{th})/RT]} \tag{1}$$

where G is the maximum channel conductance, $P_{open}(V)$ is the open state probability of the channel, V_{th} is the threshold potential, F is the Faraday constant, R is the gas constant, and T is the temperature. Since $(dP_{open}/dV)_{V_{th}} = -zF/4RT$, the parameter z gives the steepness of the transition region between the open and closed conductance states (z can be regarded as the effective number of channel charges involved in gating [5]).

To better show the electrical characteristics of Eq. (1), we rewrite the I–V and (dV/dI)–V curves introducing the dimensionless variables $\tilde{I} = I/(GV_T)$, $\tilde{V} = V/V_T$, $\tilde{V}_{th} = V_{th}/V_T$ and

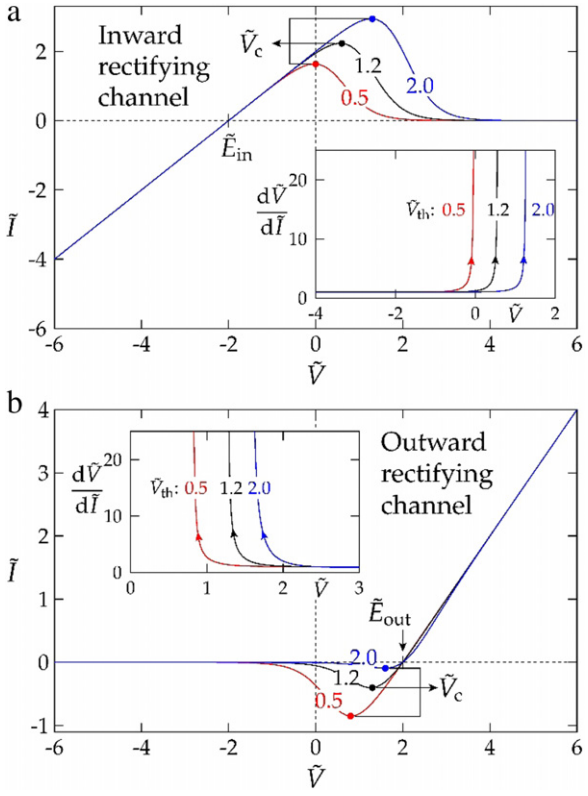

Fig. 1. (a) The characteristic current–potential curves of an inward rectifying channel obtained from Eqs. (2) and (3) in terms of dimensionless variables. The curves correspond to the threshold potential values $\tilde{V}_{th} = V_{th}/V_T = 0.5$, 1.2, and 2.0 (equivalent to $V_{th} = 13.5$, 32, and 54 mV, respectively) for a fixed equilibrium potential $\tilde{E}_{in} = E_{in}/V_T = -2$ (equivalent to $E_{in} = -54$ mV) and a gating effective charge $z = 3$ [5,16]. The inset shows $d\tilde{V}/d\tilde{I}$ as a function of $\tilde{V} < \tilde{V}_c$. This magnitude attains high values close to the critical potentials $\tilde{V}_c$ giving the maxima in the $\tilde{I}$–$\tilde{V}$ curves. The potential $\tilde{V}_c$ can then be regarded as an excitation potential [18] giving the transition between the positive and negative differential conductance of Fig. 1(a). (b) The electrical characteristics of outward rectifying channels can also be obtained from Eq. (2) changing the sign of z to $z_{out} = -3$ and replacing $\tilde{E}_{in}$ by $\tilde{E}_{out} = 2$.

$\tilde{E}_{in} = E_{in}/V_T$ (note that $V_T = RT/F = 27$ mV at $T = 310$ K):

$$\tilde{I} = (\tilde{V} - \tilde{E}_{in})P_{open}(\tilde{V}), \quad P_{open}(\tilde{V}) = \frac{1}{1 + \exp[z(\tilde{V} - \tilde{V}_{th})]} \tag{2}$$

$$\frac{d\tilde{V}}{d\tilde{I}} = \frac{\left\{1 + \exp[z(\tilde{V} - \tilde{V}_{th})]\right\}^2}{1 + \left[1 - z(\tilde{V} - \tilde{E}_{in})\right]\exp[z(\tilde{V} - \tilde{V}_{th})]}. \tag{3}$$

In Fig. 1(a), $\tilde{V} = 2$ corresponds to $V = 54$ mV ($V_T = 27$ mV at $T = 310$ K) and $\tilde{I} = 2$ to $I = 54$ pA for a channel conductance $G = 1$ nS, which are typical values for voltage-gated ion channels [18–20]. Note that outward rectification [5] can also be obtained from Eq. (2) by changing the sign of z and replacing E_{in} with a positive equilibrium potential E_{out} (see Fig. 1(b) for some examples that are considered in Section 2.5).

Note that the membrane potential can be identified with $\tilde{E}_{in}$ in Eq. (2) only because we have ignored other contributions (e.g., the sodium and chloride channels) to this potential [5,11]. The nonlinear channel conductance is high under hyperpolarization ($\tilde{V} < \tilde{E}_{in}$), favoring thus the entry of potassium ions, and decreases under depolarization ($\tilde{V} > \tilde{E}_{in}$), as shown in Fig. 1(a). This electrical rectification allows controlling the cell membrane potential by establishing a barrier to external stimuli [18].

However, it is not usual for the cell potential to become more negative than $\tilde{E}_{in}$ and it is the small outward current carried at po-

tentials more positive than $\tilde{E}_{in}$ (see Fig. 1(a)) that maintains $\tilde{V}$ close to $\tilde{E}_{in}$ [5] against external depolarizing stimuli. This stabilizing effect is operative until $\tilde{V}$ is close to the critical potential $\tilde{V}_c$ giving the maxima in the $\tilde{I}$–$\tilde{V}$ curves of Fig. 1(a). In the potential region $\tilde{V} > \tilde{V}_c$, the channel closes, entering a region of negative differential resistance ($d\tilde{V}/d\tilde{I} < 0$ in Fig. 1(a)), because of internal gating processes and the action of external blockers [5,15,18,19,21,22]. The experimental $\tilde{I}$–$\tilde{V}$ curves tend to follow the nonlinear trends of Fig. 1(a) [5,14,15,17–19,21–24] and can be obtained by applying hyperpolarizing and depolarizing potential ramps of characteristic times large enough for the channel response to be slave of input signal [20,21]. The effect of potassium concentration on the curves can be discussed in terms of $\tilde{E}_{in}$ [5,15,24].

The results of Fig. 1(a) and (b) show that the channel electrical sensitivity (i.e. the current through the channel as a response to changes in the potential $\tilde{V}$) is dictated by the threshold potential $\tilde{V}_{th}$. Therefore, spatial domains of different ion channels may permit or suppress the transmission of electrical signals over the cell surface depending of the values of this potential. In those cases where the domains are electrically coupled by a common membrane potential $\tilde{V}_m = \tilde{V}(\tilde{I} = 0)$, we will consider the potential difference $\tilde{V}_{th} - \tilde{V}_m$ as an index for the domain electrical sensitivity in the next section.

1.3. Diversity of channels and electrical domains

In complex biological systems, the observable physical magnitudes usually emerge as average values over the individual responses of many units that may show a significant diversity at the single unit level. In particular, the membrane potential constitutes an average electrical index that results from the individual activity of many ion channels and transporters with different electric characteristics localized over the cell surface domains [9,10]. The mechanisms by which neighboring domains can show locally different potentials are not completely understood [9,10] and may involve also surface potentials due to fixed charges [25]. However, it is believed that heterogeneous patches of ion channels and transporters may form a spatio-temporal map of potentials over the cell surface which supports locally different ionic fluxes relevant to developmental processes [1,4,8,10,26,27].

Because of the relevant physiological role of voltage-gated potassium channels in patterning [7,9] and their high heterogeneity [6,14,15], we now consider how the diversity of threshold voltages over the cell surface can support a map of electrical sensitivities to external bioelectric perturbations [9]. To this end, we introduce the idealization that each domain can be represented by a fixed number of channels with the same threshold potential $\tilde{V}_{th}$. However, distinct domains may still have different values of $\tilde{V}_{th}$ [16]. We use the phenomenological model for voltage gating of Fig. 1(a) because it reproduces the observed rectification characteristics [5,15] and incorporates the experimental fact that these characteristics are distinct for different types of channels [14]. (Note that, even for the same type of channels, a significant variability between the individual responses is found experimentally [23].) There exist more detailed models allowing for quantitative estimations of the cell ionic concentrations and membrane potential [28] where the state of the cell is described by a system of coupled nonlinear differential equations describing the different channels and pumps [26,28–30]. However, we assume for the sake of simplicity that the extracellular environment fixes the ionic concentrations and equilibrium potentials and ignore the concentration changes occurring for long times (note that the number of ions needed to establish typical potential differences is very small compared with the total number of ions in the cell [5]).

2. Results and discussion

In the following calculations, we have used the phenomenological equation (1) or (2) to describe the average current–voltage curve characteristic of the ion channels. In some cases indicated in the figures, however, we have simulated the time fluctuations of the current obtained for one (or a few channels) to better show the electrical response of the channels. In this case, the channel opening (conductive state) [31–33] is described by the stochastic probability $P_{open,\,stoch}(\tilde{V})$, which is evaluated using a Monte Carlo algorithm as follows. At every time step, a random number r ($0 \leq r \leq 1$) is generated from a uniform distribution and $P_{open,\,stoch}(\tilde{V})$ is assigned the value:

$$P_{open,\,stoch}(\tilde{V}) = \begin{cases} 1 & \text{if } r \leq 1/\left\{1 + \exp[z(\tilde{V} - \tilde{V}_{th})]\right\} \\ 0 & \text{if } r > 1/\left\{1 + \exp[z(\tilde{V} - \tilde{V}_{th})]\right\} \end{cases} \tag{4}$$

so that the current delivered by the channel is:

$$\tilde{I} = \begin{cases} (\tilde{V} - \tilde{E}_{in}), & \text{if the channel is open} \\ 0, & \text{if the channel is closed.} \end{cases} \tag{5}$$

The Monte Carlo approach allows implementing a channel dynamics by introducing steps of dimensionless time $\tilde{t} = t/(C/G)$ in the simulations, where C is a typical electrical capacitance of the channels. The time average of the current in Eq. (5) gives the value of the current in Eq. (2) for long enough times.

2.1. Current fluctuations in channels and threshold diversity

We study now the electrical response of three domains of voltage-gated channels composed by $N = 50$ identical channels whose characteristics are those of Fig. 1(a) (each domain is characterized by a different threshold potential). To illustrate the electrical sensitivity of the ion channels, we consider first the time fluctuations in the current trace of the domain of threshold potential $\tilde{V}_{th}$.

Fig. 2(a) shows the current traces obtained at $\tilde{V} = 0$ for three domains of different threshold potentials $\tilde{V}_{th} = 0.5$, 1.2 and 2.0. The potential $\tilde{V} = 0$ has been considered here because it is close to the critical potential $\tilde{V}_c = -0.03$ corresponding to $\tilde{V}_{th} = 0.5$ in Fig. 1(a). Fig. 2(b) shows the current traces at three potentials $\tilde{V}$ approaching the critical $\tilde{V}_c$ of the domain with $\tilde{V}_{th} = 0.5$. The electrical noise increases with decreasing $\tilde{V}_{th}$ (Fig. 2(a) at fixed $\tilde{V}$) and with increasing cell potential in the range $\tilde{V} < \tilde{V}_c$ (Fig. 2(b) at fixed $\tilde{V}_{th}$). The noise amplitudes are related with the different electrical responses characteristic of the domains, which are dictated by the particular values of $\tilde{V}_{th}$.

The results of Fig. 2(a) and (b) suggest that channel domains localized on the cell surface can show different electrical responses based on the potential $\tilde{V}_c$ (and then $\tilde{V}_{th}$). This fact is relevant for establishing electrical maps on the cell surface because of the different channel domain behavior in the limit $\tilde{V} \to \tilde{V}_c$ (see Fig. 2(a) for $\tilde{V}_c \approx 0$).

2.2. The diversity in the thresholds leads to a pattern of electrical sensitivities

We incorporate now the effects of the threshold diversity on the electrical sensitivity of different channel domains. This

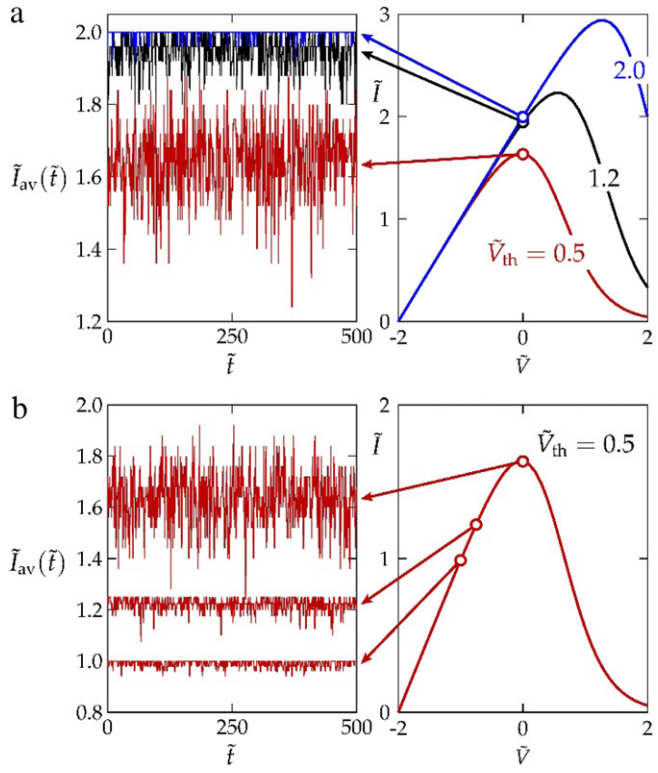

Fig. 2. (a) Dimensionless current traces $\tilde{I}_{av}(\tilde{t})$ *vs.* time $\tilde{t}$. The three traces are obtained as average values over three different domains, with $\tilde{V}_{th} = 0.5$, 1.2, and 2.0, of $N = 50$ identical channels using Monte Carlo simulations based on Eqs. (4) and (5). There is no potential difference across the channels, $\tilde{V} = 0$, which is close to the critical potential $\tilde{V}_c = -0.03$ for $\tilde{V}_{th} = 0.5$ in Fig. 1(a). (b) $\tilde{I}_{av}(\tilde{t})$ *vs.* $\tilde{t}$ obtained as average values over a domain of $N = 50$ identical channels with $\tilde{V}_{th} = 0.5$ at three cell potentials $\tilde{V} = -1, -0.75$, and 0. In all cases, $\tilde{E}_{in} = -2$ and $z = 3$, as in Fig. 1(a). The corresponding voltage $\tilde{V}$ windows in Fig. 1(a) are also shown for clarity.

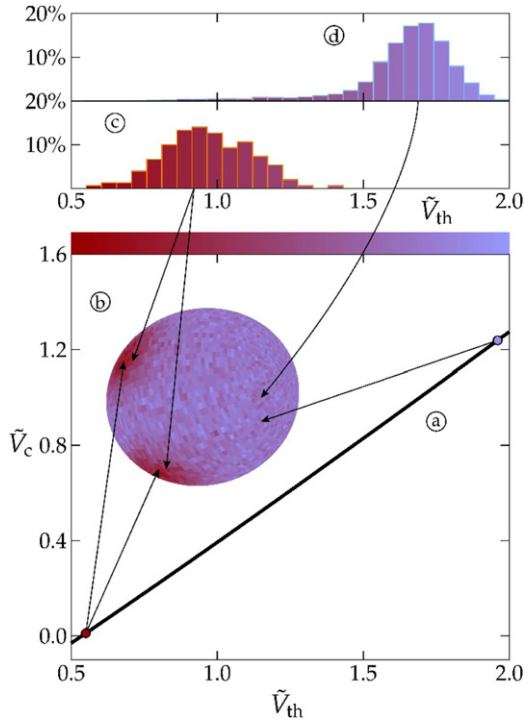

Fig. 3. The linear dependence of the critical potential $\tilde{V}_c$ on the threshold potential $\tilde{V}_{th}$ (a) for a channel characterized by Eq. (2) and Fig. 1(a) suggests that we can use $\tilde{V}_c$ or $\tilde{V}_{th}$ to assess the electrical sensitivity of the channel. Considering two spatial locations on the membrane surface (b), two different Gauss distributions of low (c) and high (d) threshold potentials are introduced. A gradient color scale is assigned to $\tilde{V}_{th}$ between the lowest value $\tilde{V}_{th} = 0.5$ (dark color) in the threshold distribution (c) and the highest value $\tilde{V}_{th} = 2.0$ (light color) in the distribution (d). Because a low $\tilde{V}_{th}$ value gives a low $\tilde{V}_c$ value (and then a high electrical sensitivity), the dark colors over the membrane surface (b) show the regions with higher sensitivity to changes in the potential. The arrows show the spatial regions on the cell surface where the low and high threshold distribution domains are assumed to be localized. Two particular values of $\tilde{V}_c$ characteristic of the different surface domains in the regions (bottom inset) are also shown. (For interpretation of the references to color in this figure legend, the reader is referred to the web version of this article.)

diversity originates from the individual heterogeneity in the geometry and charge distributions of the channels, which results in statistical distributions for the threshold potential $\tilde{V}_{th}$ characterized by central and width distribution values (central inset of Fig. 3) [14,16,23]. These types of distributions are significant not only for biological pores [16,23] but also for artificial threshold nanostructures such as field-effect nanowires, carbon nanotubes, and single electron transistors [34].

Fig. 1(a) showed the relevance of the critical potential $\tilde{V}_c$ for the channel electrical response [18]. The potential $\tilde{V}_c$ corresponds to the maximum value of $\tilde{I}$ in Fig. 1(a) at each threshold potential $\tilde{V}_{th}$ and can be obtained from Eq. (3) imposing that the denominator vanishes at $\tilde{V}_c$, $1 + [1 - z(\tilde{V}_c - \tilde{E}_{in})] \exp[z(\tilde{V}_c - \tilde{V}_{th})] = 0$. This equation can be readily solved for $\tilde{V}_{th}$ as $\tilde{V}_{th} = \tilde{V}_c + \ln[z(\tilde{V}_c - \tilde{E}_{in}) - 1]/z$. If we consider the results of Fig. 1(a), where $\tilde{E}_{in} = -2$ and $z = 3$, the first term of the right hand side, $\tilde{V}_c$, varies between $\tilde{V}_c = -0.03$ ($\tilde{V}_{th} = 0.5$) and $\tilde{V}_c = 1.28$ ($\tilde{V}_{th} = 2.0$), whereas the second term of the equation varies more slowly from 0.53 to 0.73. This means that the dependence between $\tilde{V}_c$ and $\tilde{V}_{th}$ is almost linear, as shown in Fig. 3. In addition, this fact suggests that we can use $\tilde{V}_c$ or $\tilde{V}_{th}$ to assess the electrical sensitivity of the channel.

We consider two heterogeneous domains of non-identical channels in Fig. 3. The domains are described by two different Gaussian distributions of low (c) and high (d) threshold potentials (central inset) instead of by a single value of $\tilde{V}_{th}$. We assume that the domains are localized on three spatial regions of the cell surface (bottom inset). $N_1 = 150$ low threshold channels (distribution 1) are spatially restricted on each of the two small (dark colored) regions while $N_2 = 6100$ high threshold channels (distribution 2) are spread over the dominant (light colored) region. The maximum electrical sensitivity corresponds to the lowest value of $\tilde{V}_{th}$ in the two domains characterized by distribution 1 while the minimum sensitivity corresponds to the highest value of $\tilde{V}_{th}$ in the domain characterized by distribution 2. Fig. 3 shows that a map of threshold potentials (central inset) can be translated into spatial domains (bottom inset) of different electrical sensitivities (top inset).

2.3. Leak conductance and threshold diversity

Fig. 3 suggests that heterogeneous domains characterized by channels with different thresholds can support domains of different electrical sensitivities over the cell surface. However, the question of the nonlinear coupling between currents and potentials still remains to be addressed. A direct extension of the above model considers leaky Ohmic channels in parallel with voltage-gated channels [23,32]. The leaky channels have a linear current (I_L)–potential (V) response:

$$I_L = G_L(V - E_L) \tag{6}$$

where G_L is the channel conductance and E_L is a characteristic potential [23] (examples of leaky channels and their influence on membrane potential can be found in Refs. [5,23,32]). For simplicity, we consider a homogeneous domain with N_L leaky

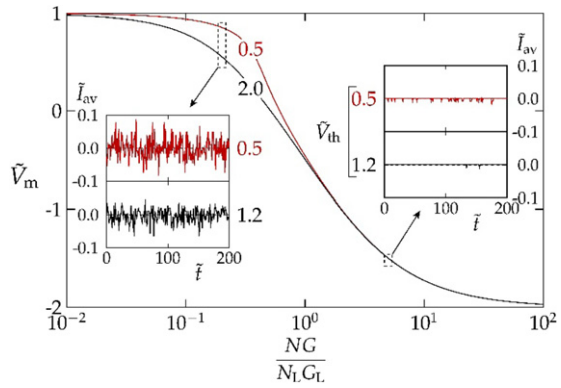

Fig. 4. The membrane potential $\tilde{V}_m$ of an isolated domain *vs.* the ratio of the total channel and leak conductances, $NG/(N_L G_L)$, is shown for two domains of threshold potentials $\tilde{V}_{th} = 0.5$ (top curve) and 1.2. Each curve is obtained from Eq. (7) for N voltage-gated channels with the same $\tilde{V}_{th}$ in parallel with N_L identical leaky channels. The insets show the current $\tilde{I}_{av}(\tilde{t})$ around $\tilde{I}_{av} = 0$ *vs.* time $\tilde{t}$ in the different regimes where the leaky or the voltage-gated channels dominate the ionic conduction. The currents are average values obtained with $N = 50$ channels by means of Monte Carlo simulations considering the stochastic opening and closing of the channels (see Fig. 2(a)). In all cases, $\tilde{E}_{in} = -2$ and $z = 3$, as in Fig. 1, and $\tilde{E}_L = 1$.

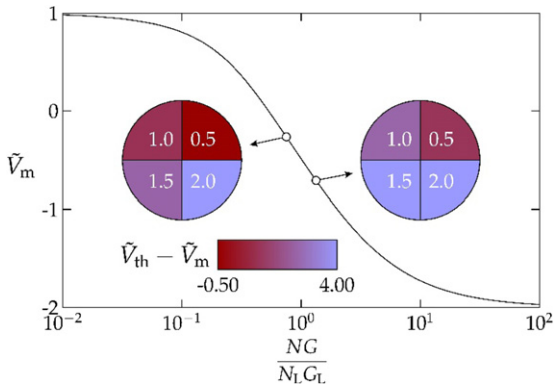

Fig. 5. The membrane potential $\tilde{V}_m$ *vs.* the ratio $NG/(N_L G_L)$ is shown for the case of four electrically coupled homogeneous domains with characteristic threshold potentials 0.5, 1.0, 1.5, and 2.0. The curve is obtained from Eq. (8) for $\tilde{E}_{in} = -2$, $z = 3$, and $\tilde{E}_L = 1$, as in Fig. 4. Each of the four domains (circular sectors in the insets) is composed of N voltage-gated channels with the same $\tilde{V}_{th,i}$ (i = 1, 2, 3, and 4) in parallel with N_L identical leaky channels. The two circular insets correspond to the particular values of $\tilde{V}_m$ marked by the arrows. The different colors in the horizontal scale of the inset refer to the value of $\tilde{V}_{th}$–$\tilde{V}_m$ characteristic of each domain. (For interpretation of the references to color in this figure legend, the reader is referred to the web version of this article.)

channels of the same conductance G_L and potential E_L in parallel with N identical voltage-gated channels of threshold potential V_{th}, maximum conductance G, and equilibrium potential E_{in}. The (zero current) membrane potential of an isolated domain can now be obtained from the condition $N_L I_L + NI = 0$, where $N_L I_L$ is the total leakage current. In terms of dimensionless variables, this condition gives an equation for the membrane potential $\tilde{V}_m = \tilde{V}(\tilde{I} = 0)$ of the domain:

$$\tilde{V}_m - \tilde{E}_L + \frac{NG}{N_L G_L}(\tilde{V}_m - \tilde{E}_{in})\frac{1}{1 + \exp[z(\tilde{V}_m - \tilde{V}_{th})]} = 0. \tag{7}$$

This equation can be solved to give $NG/(N_L G_L)$ as a function of $\tilde{V}_m$.

Fig. 4 shows the membrane potential $\tilde{V}_m$ of two isolated domains vs. the ratio $NG/(N_L G_L)$ parametrically in the threshold potential $\tilde{V}_{th}$ of each domain. The insets show the current traces around the average value $\tilde{I}_{av} = 0$ in the limits $NG/(N_L G_L) \ll 1$ (the leaky channels dominate conduction and then $\tilde{V}_m \approx \tilde{E}_L$) and $NG/(N_L G_L) \gg 1$ (the voltage-gated channels dominate conduction and then $\tilde{V}_m \approx \tilde{E}_{in}$). Note that the deviation between the curves obtained for the two domains of different threshold potentials is noticeable only in the potential region $\tilde{V} > 0$ of Fig. 1(a) where the effect of $\tilde{V}_{th}$ on conduction is significant. The current fluctuations are also important in this limit (insets of Fig. 4), especially in the case of the low threshold domain, in agreement with the results of Fig. 2(a). Indeed, if we compare the fluctuations shown in the insets, we observe that they are high when $\tilde{V}_m$ is close to $\tilde{V}_{th}$ (and then to $\tilde{V}_c$). Fig. 4 shows that a map of threshold potentials can give different electrical sensitivities also when leaky channels are present.

2.4. One single membrane potential, a multiplicity of domain electrical sensitivities

We demonstrate now that a single value of the membrane potential can correspond to a multiplicity of local electrical sensitivities over different channel domains. To this end, we consider the coupling between the currents of four homogeneous domains characterized by the threshold potentials 0.5, 1.0, 1.5, and 2.0. We assume for simplicity that all channels have the same equilibrium potential $\tilde{E}_{in}$, gating charge $z = 3$, and maximum conductance G. As in the above section, each domain is composed of N identical voltage-gated channels [23,32] in parallel with N_L identical leaky channels of conductance G_L and potential E_L. From the condition of zero total current, the membrane potential $\tilde{V}_m$ common to the four electrically coupled homogeneous domains is obtained from the equation:

$$\tilde{V}_m - \tilde{E}_L + \frac{NG}{N_L G_L}(\tilde{V}_m - \tilde{E}_{in}) \times \frac{1}{4}\sum_{i=1}^{4}\frac{1}{1 + \exp[z(\tilde{V}_m - \tilde{V}_{th,i})]} = 0 \tag{8}$$

which is a generalization of Eq. (7).

Fig. 5 shows $\tilde{V}_m$ as a function of the ratio $NG/(N_L G_L)$. The inset gives the map of the domain electrical sensitivities, described now by the potential difference $\tilde{V}_{th,i}$–$\tilde{V}_m$, on a color scale. The difference $\tilde{V}_{th,i}$–$\tilde{V}_m$ measures the distance between the threshold potential $\tilde{V}_{th,i}$ characteristic of a given domain and the membrane potential $\tilde{V}_m$ common to all domains. Note that this difference dictates the closure potential window characteristic of a particular inward rectifying channel (see the denominator in the sum of Eq. (8)), controlling then the stability and fluctuations of the membrane potential.

Channel closure is more likely to occur over the dark colored domains (low $\tilde{V}_{th}$–$\tilde{V}_m$ values) of Fig. 5 because they are more sensitive to external electrical signals (see Fig. 1(a); note that channel closure does not allow the stabilization of the membrane potential at the value $\tilde{E}_{in}$ in Fig. 1(a)). This result shows again that the parameter $\tilde{V}_{th}$–$\tilde{V}_m$ is useful to understand basic functions of the channel, although other feedback mechanisms such as the ion pumps and additional channels [26,28–30] should also participate in the electrical coupling for a complete description of the problem.

2.5. The case of two voltage-gated ion channels acting simultaneously

A multiplicity of electrically coupled channels should exist over the cell membrane [26,28–30]. The case of two distinct voltage-gated ion channels with different rectifying properties and different Nernst equilibrium potentials $\tilde{E}_{in}$ and $\tilde{E}_{out}$ (Fig. 1(a) and (b)) constitutes a significant extension of the previous results.

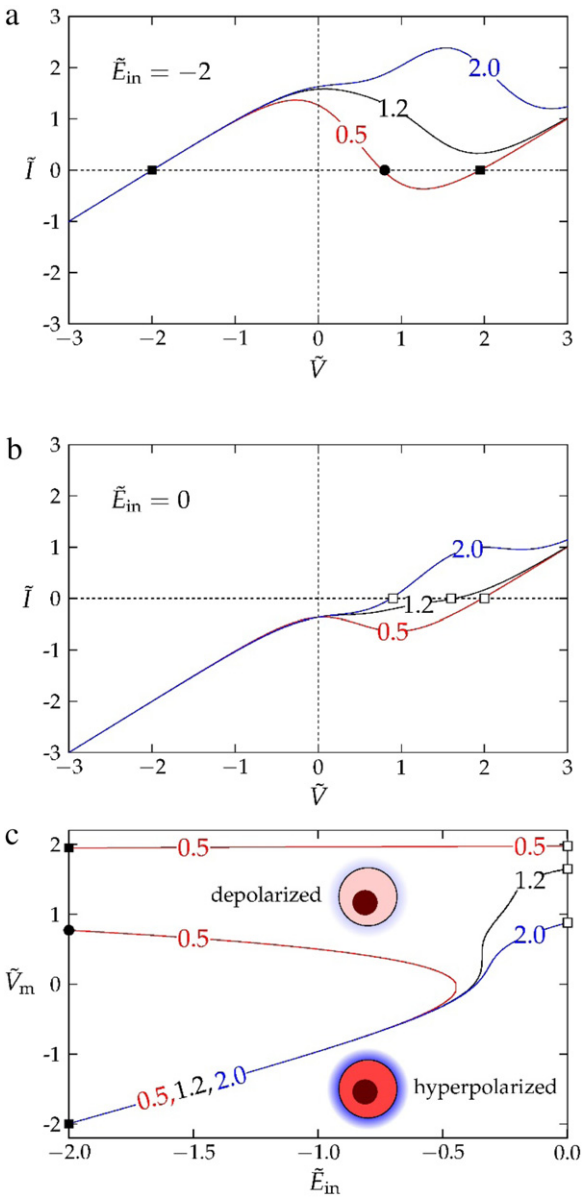

Fig. 6. Total current $\tilde{I} = \tilde{I}_{in} + \tilde{I}_{out}$ *vs.* $\tilde{V}$ for two generic inward (*in*) and outward (*out*) rectifying channels in the cases $\tilde{E}_{in} = -2.0$ (a) and $\tilde{E}_{in} = 0$ (b). The curves are parametric in the threshold potential $\tilde{V}_{th,in}$ and have been obtained with $z_{in} = -z_{out} = 3$, $G_{in} = G_{out}$, $\tilde{E}_{out} = 2$ and $\tilde{V}_{th,out} = 0.5$. The membrane potential at zero current ($\tilde{V}_m$) *vs.* $\tilde{E}_{in}$ is shown for the same system parameters of Fig. 6(a) and (b) (c). Note the correspondence between the marked points in Fig. 6(a)–(c). The curve corresponding to $\tilde{V}_{th,in} = 0.8$ is included in Fig. 6(c) to better show the onset of bistability effects.

Figs. 6(a) and (b) show the total current $\tilde{I} = \tilde{I}_{in} + \tilde{I}_{out}$ of inward (*in*) and outward (*out*) rectifying channels for three threshold potentials $\tilde{V}_{th,in}$ (the numbers in the curves). The curves are parametric in the threshold potential $\tilde{V}_{th,in}$ and have been obtained with $z_{in} = -z_{out} = 3$, $G_{in} = G_{out}$, $\tilde{E}_{out} = 2$ and $\tilde{V}_{th,out} = 0.5$. Figs. 6(a) and 6(b) are obtained at the equilibrium potentials $\tilde{E}_{in} = -2.0$ and 0, respectively.

Remarkably, Fig. 6(c) shows that the coupled channels can lead to a multiplicity of membrane potentials $\tilde{V}_m$ for the lower threshold potential $\tilde{V}_{th,in} = 0.5$ at sufficiently high (in absolute value) equilibrium potentials $\tilde{E}_{in}$. Indeed, Fig. 6(a) shows that there is an unstable point (central circle) between two stable points (squares) corresponding here to negative and positive potentials [35]. The above results arise from the central region of negative differential conductance in Fig. 6(a). Note also that the membrane potential $\tilde{V}_m$ is not very sensitive to the threshold potential $\tilde{V}_{th,in}$ for large (in absolute value) negative potentials $\tilde{E}_{in}$ and $\tilde{V}_m$. When $\tilde{E}_{in}$ tends to zero, $\tilde{V}_m$ depends on the threshold potential $\tilde{V}_{th,in}$, showing bistability for $\tilde{V}_{th,in} = 0.5$ in Fig. 6(c).

Consider $\tilde{E}_{in} = -2.0$ in the curve for $\tilde{V}_{th,in} = 0.5$ of Fig. 6(c). Eq. (1) shows that the stable membrane potential $\tilde{V}_m = -2.0$ corresponds to individually zero channel currents, $\tilde{I}_{in} = 0 = \tilde{I}_{out}$. The inward channel with $\tilde{E}_{in} = -2.0$ and $z_{in} = 3$ is at the equilibrium potential (see Fig. 1(a)) while the outward channel with $\tilde{E}_{out} = 2.0$ and $z_{out} = -3$ is closed (see Fig. 1(b)). The two other cases correspond to current compensation between the inward and outward channels. The stable potential $\tilde{V}_m = 1.9$ is close to the equilibrium potential of the outward channel ($\tilde{E}_{out} = 2.0$) and corresponds to lower inward and outward currents than the unstable potential $\tilde{V}_m = 0.8$ (see Fig. 1(a) and (b)).

When externally perturbed, the membrane potential $\tilde{V}_m$ should eventually reach one of the stable points [35] along the top and bottom curves with $\tilde{V}_{th,in} = 0.5$ in Fig. 6(c). We will not pursue this question further because other elements ignored in the model such as ion pumps and transporters [26,28–30] may influence the system response. We must mention, however, that *N*-shaped current–voltage curves (see Fig. 6(a) and (b)) and membrane potential bistability (see Fig. 6(c)) have been confirmed experimentally and theoretically at low extracellular potassium concentration [36] (note that the potential $\tilde{E}_{in}$ in the axis of Fig. 6(c) depends on this concentration [5]). Individual skeletal [36] and mouse lumbrical [30] muscle cells have experimentally shown membrane potential bistability. Also, the resting membrane potential of the hair cell membrane has been found to fluctuate between two values determined by the potential region characteristic of the low membrane conductance range [37]. In all the above cases, inward rectifying potassium channels played a crucial role in the observed bistability phenomena [30,36,37].

3. Conclusions

In non-neural cells, the changes in the electrical potentials characteristic of the cell cycle are regulated by the nonlinear conductance of ion channels localized over different domains on the surface membrane. In particular, voltage-gated potassium channels are involved in the cell hyperpolarization and depolarization processes that control electrical signals and ionic currents. These channels constitute a good candidate to study basic biological questions on a more simplified scale than the complete cell membrane. Also, the channels show a significant heterogeneity, making it possible to analyze the effects of diversity in the electrical responses of different channel domains. We have considered a phenomenological model of potassium inward rectifying channels (see Fig. 1(a)), showing that the diversity of threshold potentials could be related with the establishment of spatial domains with different electrical responses over a model cell surface (see Figs. 2 and 3). Although the physical model is a crude picture of the biological problem in the sense the above channels alone are not sufficient to explain the intricate mutual influence of concentrations and potentials, inward rectifying channels play a key role in membrane depolarization [5,38] because they dictate the potassium permeability of many cells. Therefore, considering these channels with detail should constitute a first step to the incorporation of other elements and mechanisms (e.g. the coupling of potassium and sodium channels with ion pumps and the activity of calcium channels) needed for a complete description of this highly nonlinear problem.

The membrane potential of a cell obtained by standard electrophysiological methods is only an average electrical magnitude [4,5,9,10]. The simple models considered here also explore the connection of this magnitude with surface patches of ion channels (domains) having locally different electrical properties (see Figs. 4 and 5). These spatial domains may permit or suppress the transmission of electrical signals according to their particular responses to external electric signals. Note also that much emphasis is usually put on the quasi-steady state values of cell membrane potentials while the present results offer some clues to the understanding of the transition between the different potential values (see Figs. 4–6). Indeed, depolarization shifts the potential $\tilde{V}$ to less negative values in Fig. 1(a), entering the channel into the region of potentials close to $\tilde{V}_c$ where it can no longer control the cell membrane potential against the external stimuli [5,15,18] and other fluctuations [39,40]. In the limiting case of channel closure, the stabilization of the membrane potential is not possible [5]. The potential range over which the channel controls the membrane potential is dictated by the gating steepness in Fig. 1(a) [5], which depends on the critical potential $\tilde{V}_c$ (and then on the threshold potential $\tilde{V}_{th}$ in Fig. 3). The results of Fig. 5 suggest that channel closure and depolarization are more likely to occur over spatial domains of high sensitivity to external bioelectrical signals (low values of $\tilde{V}_{th}$ and $\tilde{V}_{th}-\tilde{V}_m$), being unlikely for low sensitivity domains (high values of $\tilde{V}_{th}$ and $\tilde{V}_{th}-\tilde{V}_m$). The experimental interdependence between $\tilde{V}_{th}$ and $\tilde{V}_m$ [23] and the crucial role of the channel gating for controlling the cell cycle [6] have previously been noted. Also, the nonlinear electrical coupling of channels with different threshold potentials can lead to a rich variety of bioelectrical phenomena, including regions of membrane potential bi-stability (see Fig. 6).

Acknowledgments

We acknowledge the financial support from the Ministry of Economic Affairs and Competitiveness and FEDER (project MAT2012-32084), and the Generalitat Valenciana (project PROMETEO/GV/0069).

References

[1] M. Olivotto, A. Arcangeli, M. Carla, E. Wanke, Electric field at the plasma membrane level: a neglected element in the mechanisms of cell signaling, BioEssays 18 (1996) 495–504.
[2] C.D. Mccaig, A.M. Rajnicek, B. Song, M. Zhao, Controlling cell behavior electrically: Current views and future potential, Physiol. Rev. 85 (2005) 943–978.
[3] C.D. Mccaig, B. Song, A.M. Rajnicek, Electrical dimensions in cell science, J. Cell Sci. 122 (2009) 4267–4276.
[4] M. Levin, Molecular bioelectricity in developmental biology: New tools and recent discoveries. Control of cell behavior and pattern formation by transmembrane potential gradients, BioEssays 34 (2012) 205–217.
[5] B. Hille, Ion Channels of Excitable Membranes, third ed., Sinauer Associates, Sunderland, 1992.
[6] D. Urrego, A.P. Tomczak, F. Zahed, W. Stühmer, L.A. Pardo, Potassium channels in cell cycle and cell proliferation, Philos. Trans. R. Soc. B 369 (2014) 20130094.
[7] G.R. Dahal, J. Rawson, B. Gassaway, B. Kwok, Y. Tong, L.J. Ptácek, E. Bates, An inwardly rectifying K^+ channel is required for patterning, Development 139 (2012) 3653–3664.
[8] R. Shi, R.B. Borgens, Three-dimensional gradients of voltage during development of the nervous system as invisible coordinates for the establishment of embryonic pattern, Dev. Dyn. 202 (1995) 101–114.
[9] M. Levin, Large-scale biophysics: ion flows and regeneration, Trends Cell Biol. 17 (2007) 262–270.
[10] D.S. Adams, M. Levin, Endogenous voltage gradients as mediators of cell–cell communication: strategies for investigating bioelectrical signals during pattern formation, Cell Tissue Res. 352 (2013) 95–122.
[11] M. Yang, W.J. Brackenbury, Membrane potential and cancer progression, Front. Physiol. 4 (2013) 185.
[12] J.L. Fiske, V.P. Fomin, M.L. Brown, R.L. Duncan, R.A. Sikes, Voltage-sensitive ion channels and cancer, Cancer Metastasis Rev. 25 (2006) 493–500.
[13] S. Perathoner, J.M. Daane, U. Henrion, G. Seebohm, C.W. Higdon, S.L. Johnson, C. Nüsslein-Volhard, M.P. Harris, Bioelectric signaling regulates size in zebrafishc fins, PLoS Genet. 10 (2014) e1004080.
[14] J.M.B. Anumonwo, A.N. Lopatin, Cardiac strong inward rectifier potassium channels, J. Mol. Cell Cardiol. 48 (2010) 45–54.
[15] Z. Lu, Mechanism of rectification in inward-rectifier K^+ channels, Annu. Rev. Physiol. 66 (2004) 103–129.
[16] J. Cervera, S. Mafe, Threshold diversity effects on the electric currents of voltage-gated ion channels, Europhys. Lett. EPL 102 (2013) 68002.
[17] E.A. Newman, Inward-rectifying potassium channels in retinal glial (Müller) cells, J. Neurosci. 13 (1993) 3333–3345.
[18] D. Oliver, T. Baukrowitz, B. Fakler, Polyamines as gating molecules of inward-rectifier K1 channels, Eur. J. Biochem. 267 (2000) 5824–5829.
[19] B. Fakler, U. Bdindle, E. Glowatzki, S. Weidemann, H.-P. Zenner, J.P. Ruppersberg, Strong voltage-dependent inward rectification of inward rectifier K^+ channels is caused by intracellular spermine, Cell 80 (1995) 149–154.
[20] M. Queralt-Martin, E. Garcia-Gimenez, V.M. Aguilella, P. Ramirez, S. Mafe, A. Alcaraz, Electrical pumping of potassium ions against an external concentration gradient in a biological ion channel, Appl. Phys. Lett. 103 (2013) 043707.
[21] N. von Beckerath, M. Dittrich, H.-G. Klieber, J. Daut, Inwardly rectifying K^+ channels in freshly dissociated coronary endothelial cells from guinea-pig heart, J. Physiol. 491 (2) (1996) 357–365.
[22] B.K. Panama, A.N. Lopatin, Differential polyamine sensitivity in inwardly rectifying Kir2 potassium channels, J. Physiol. 571 (2006) 287–302.
[23] A. Arcangeli, L. Bianchi, A. Becchetti, L. Faravelli, M. Coronnello, E. Mini, M. Olivotto, E. Wanke, A novel inward-rectifying K^+ current with a cell-cycle dependence governs the resting potential of mammalian neuroblastoma cells, J. Physiol. 489 (2) (1995) 455–471.
[24] W. Tang, X.-C. Yang, Cloning a novel human brain inward rectifier potassium channel and its functional expression in Xenopus oocytes, FEBS Lett. 348 (1994) 239–243.
[25] V.M. Aguilella, S. Mafé, J.A. Manzanares, Double layer potential and degree of dissociation in charged lipid monolayers, Chem. Phys. Lipid 105 (2000) 225–229.
[26] M. Léonetti, E. Dubois-Violette, F. Homblé, Pattern formation of stationary transcellular ionic currents in Fucus, PNAS 101 (2004) 10243–10248.
[27] D. Kline, K.R. Robinson, R. Nuccitelli, Ion currents and membrane domains in the cleaving Xenopus egg, J. Cell Biol. 97 (1983) 1753–1761.
[28] J.A. Fraser, C.L.-H. Huang, Quantitative techniques for steady-state calculation and dynamic integrated modelling of membrane potential and intracellular ion concentrations, Prog. Biophys. Mol. Biol. 94 (2007) 336–372.
[29] V. Jacquemet, Steady-state solutions in mathematical models of atrial cell electrophysiology and their stability, Math. Biosci. 208 (2007) 241–269.
[30] J. Gallahera, M. Biera, J.S. van Heukelom, First order phase transition and hysteresis in a cell's maintenance of the membrane potential—an essential role for the inward potassium rectifiers, Biosystems 101 (2010) 149–155.
[31] J.A. White, J.T. Rubinstein, A.R. Kay, Channel noise in neurons, Trends Neurosci. 23 (2000) 131–137.
[32] H. Salman, E. Braun, Voltage dynamics of single-type voltage-gated ion-channel protein ensembles, Phys. Rev. E 56 (1997) 852–864.
[33] S. Marom, H. Salman, V. Lyakhov, E. Braun, Effects of density and gating of delayed-rectifier potassium channels on resting membrane potential and its fluctuations, J. Membr. Biol. 154 (1996) 267–274.
[34] J. Cervera, J. Claver, S. Mafe, Individual variability and average reliability in parallel networks of heterogeneous biological and artificial nanostructures, IEEE Trans. Nanotechnol. 12 (2013) 1198–1205.
[35] M. Léonetti, On biomembrane electrodiffusive models, Eur. Phys. J. B 2 (1998) 325–340.
[36] H. van Mila, J.S. van Heukelom, M. Bier, A bistable membrane potential at low extracellular potassium concentration, Biophys. Chem. 106 (2003) 15–21.
[37] F. Jørgensen, A.B.A. Kroese, Ion channel regulation of the dynamical instability of the resting membrane potential in saccular hair cells of the green frog (Rana esculenta), Acta Physiol. Scand. 185 (2005) 271–290.
[38] J.S. van Heukelom, The role of the potassium inward rectifier in defining cell membrane potentials in low potassium media, analyzed by computer simulation, Biophys. Chem. 50 (1994) 345–360.
[39] J.A. Fay, Thermal fluctuations of electric field and solute density in biological cells, Phys. Rev. E 56 (1997) 3460–3467.
[40] J. Procopio, J.A. Fornés, Fluctuation–dissipation theorem imposes high-voltage fluctuations in biological ionic channels, Phys. Rev. E 51 (1995) 829–831.